Original Article

MOLECULAR METABOLISM

Iron aggravates hepatic insulin resistance in the absence of inflammation in a novel db/db mouse model with iron overload

Sandro Altamura [1,2], Katja Müdder [1], Andrea Schlotterer [3,4], Thomas Fleming [5,6], Elena Heidenreich [7], Ruiyue Qiu [1], Hans-Peter Hammes [3,4], Peter Nawroth [5,6,8], Martina U. Muckenthaler [1,2,*]

ABSTRACT

Objective: The molecular pathogenesis of late complications associated with type 2 diabetes mellitus (T2DM) is not yet fully understood. While high glucose levels indicated by increased HbA1c only poorly explain disease progression and late complications, a pro-inflammatory status, oxidative stress, and reactive metabolites generated by metabolic processes were postulated to be involved. Individuals with metabolic syndrome (MetS) frequently progress to T2DM, whereby 70% of patients with T2DM show non-alcoholic fatty liver disease (NAFLD), the hepatic manifestation of MetS, and insulin resistance (IR). Epidemiological studies have shown that T2DM and steatosis are associated with alterations in iron metabolism and hepatic iron accumulation. Excess free iron triggers oxidative stress and a switch towards a macrophage pro-inflammatory status. However, so far it remains unclear whether hepatic iron accumulation plays a causative role in the generation of IR and T2DM or whether it is merely a manifestation of altered hepatic metabolism. To address this open question, we generated and characterized a mouse model of T2DM with IR, steatosis, and iron overload.

Methods: $Lepr^{db/db}$ mice hallmarked by T2DM, IR and steatosis were crossed with $Fpn^{wt/C326S}$ mice with systemic iron overload to generate $Lepr^{db/db}/Fpn^{wt/C326S}$ mice. The resulting progeny was characterized for major diabetic and iron-related parameters.

Results: We demonstrated that features associated with T2DM in $Lepr^{db/db}$ mice, such as obesity, steatosis, or IR, reduce the degree of tissue iron overload in $Fpn^{wt/C326S}$ mice, suggesting an 'iron resistance' phenotype. Conversely, we observed increased serum iron levels that strongly exceeded those in the iron-overloaded $Fpn^{wt/C326S}$ mice. Increased hepatic iron levels induced oxidative stress and lipid peroxidation and aggravated IR, as indicated by diminished IRS1 phosphorylation and AKT activation. Additionally, in the liver, we observed gene response patterns indicative of *de novo* lipogenesis and increased gluconeogenesis as well as elevated free glucose levels. Finally, we showed that iron overload in $Lepr^{db/db}/Fpn^{wt/C326S}$ mice enhances microvascular complications observed in retinopathy, suggesting that iron accumulation can enhance diabetic late complications associated with the liver and the eye.

Conclusion: Taken together, our data show that iron causes the worsening of symptoms associated with the MetS and T2DM. These findings imply that iron depletion strategies together with anti-diabetic drugs may ameliorate IR and diabetic late complications.

Keywords NAFLD; Insulin resistance; Iron; Hepcidin

1. INTRODUCTION

Patients with Metabolic Syndrome (MetS) are hallmarked by metabolic alterations that significantly increase the risk of developing type 2 diabetes mellitus (T2DM), stroke, and cardiovascular disease. To date, five risk factors have been included in the definition of MetS: abdominal obesity, hypertension, hypertriglyceridemia, low HDL cholesterol, and increased fasting blood glucose as a consequence of insulin resistance (IR). The most recent guidelines state that the simultaneous presence of three out of five risk factors is sufficient for diagnosis of MetS [1]. According to the international diabetes foundation, about 25% of the world population suffers of MetS [1,2] and its

[1]Department of Pediatric Hematology, Oncology and Immunology - University of Heidelberg, Heidelberg, Germany [2]Molecular Medicine Partnership Unit, Heidelberg, Germany [3]Fifth Medical Department - Medical Faculty Mannheim, University of Heidelberg, Heidelberg, Germany [4]European Center of Angioscience (ECAS) - Medical Faculty Mannheim, University of Heidelberg, Heidelberg, Germany [5]Department of Internal Medicine I and Clinical Chemistry, University of Heidelberg, Heidelberg, Germany [6]German Center for Diabetes Research (DZD), Neuherberg, Germany [7]Centre for Organismal Studies (COS), University of Heidelberg, Heidelberg, Germany [8]Institute for Diabetes and Cancer at Helmholtz Zentrum Munich, Neuherberg, Germany

*Corresponding author. Department of Pediatric Hematology, Oncology and Immunology - University of Heidelberg, Heidelberg, Germany. Fax: +496221564580. E-mail: martina.muckenthaler@med.uni-heidelberg.de (M.U. Muckenthaler).

Abbreviations: CRP, C-reactive protein; DIOS, dysmetabolic iron overload syndrome; DR, diabetic retinopathy; Fpn, Ferroportin; HH, hereditary hemochromatosis; IR, Insulin Resistance; IRE, Iron Responsive Element; IRP, Iron Regulatory Protein; MetS, Metabolic Syndrome; NAFLD, Non Alcoholic Fatty Liver Disease; NASH, Non Alcoholic Steatohepatitis; NTBI, Non Transferrin Bound Iron; ROS, reactive oxygen species; SEM, standard error of the mean; T2DM, Type 2 Diabetes Mellitus

Received February 5, 2021 • Revision received March 31, 2021 • Accepted April 9, 2021 • Available online 16 April 2021

https://doi.org/10.1016/j.molmet.2021.101235

prevalence increases with age and body mass index [3] and the spreading of the western lifestyle, creating a serious burden for our health systems [4–6].

T2DM is one of the most common consequences of MetS and is characterized by a combination of obesity, IR, and hyperglycemia [7]. T2DM arises when insulin secretion from pancreatic beta islets cannot be sufficiently increased to compensate for IR, resulting in hyperglycemia. In the recent years, it became evident that this definition of T2DM is rather limited since blood glucose levels per se cannot really explain the aggressiveness of the disease in terms of generation of diabetic late complications. In a subgroup of patients, diabetic-related complications such as diabetic nephropathy and retinopathy arise already at the pre-diabetes stage, before the clinical manifestations of T2DM [8,9]. Further studies have shown that diabetic retinopathy (DR) can also occur in patients with no or minor glucose abnormalities [10]. Moreover, clinical investigations demonstrated that pharmacological strategies that are able to reduce blood glucose and thus glycated hemoglobin (HbA1c) levels, only partially mitigate the risk of development of late T2DM complications. A 7.5% HbA1c level has been identified as a threshold value under which there is a little or moderate risk for the development of diabetic complications [9,11]. This demonstrates that in patients with T2DM with optimal glycemic control, the disease can still progress, suggesting that additional factors other than glucose can contribute to the diabetic-related pathologies. T2DM is associated with a pro-inflammatory state, reactive oxygen species (ROS) production and the generation of reactive metabolites such as CML, MG, and dicarbonyls. Despite these evidences, however, the molecular causes that lead to T2DM are not yet fully understood.

The liver plays an important role in the etiology of T2DM. It synthetizes and secretes two important metabolic products whose levels are altered in this disorder: glucose via glycogenolysis and gluconeogenesis, and triglycerides via *de novo* lipogenesis and very low dense lipoprotein export. Almost 80% of MetS and 70% of patients with T2DM show hepatic steatosis, the deposition of fatty acids in the liver [12–14]. This condition is defined as non-alcoholic fatty liver disease (NAFLD) and can be considered as the hepatic manifestation of MetS, IR, and T2DM [15].

Epidemiological studies have shown that hepatic fatty acid deposition is associated with alterations in iron-related parameters, a condition defined as dysmetabolic iron overload syndrome (DIOS) [16–18]. DIOS is characterized by relatively mild hepatic and body iron accumulation, moderately increased transferrin saturation, and hyperferritinemia [19]. Increased iron levels are a critical inducer of both oxidative stress and a proinflammatory state [20]. An excess of free ferrous iron triggers, via Fenton chemistry, the generation of ROS [21]. Furthermore, iron accumulation in macrophages induces oxidative stress and a proinflammatory cell state [22]. An excess of free iron aggravates atherosclerosis, a common T2DM late complication, while iron depletion can ameliorate the phenotype [23]. Therefore, iron may be an additional factor contributing, independently to glycemic levels, to T2DM progression, and the generation of diabetic late complications. In this study, we investigated the consequences of elevated systemic iron levels as a 'second hit' observed in patients with T2DM on late complication of the liver and the retina.

Body iron content is maintained at physiological levels via the hepcidin/ferroportin regulatory system. The peptide hormone hepcidin is produced by the liver in response to increased iron levels or inflammation. Its role is to limit the amount of iron exported into the bloodstream by inducing the internalization and degradation of the only known iron exporter ferroportin (Fpn), mainly expressed on iron-recycling macrophages, duodenal enterocytes and hepatocytes [24]. Disruption of the hepcidin/ferroportin interaction is the hallmark of hereditary hemochromatosis (HH) and results in unregulated iron export causing systemic and tissue iron overload. A representative mutation of HH type 4 was identified in Fpn (Fpn p.C326S) in a family affected by severe iron accumulation [25,26]. A knock-in mouse model for this mutation was recently generated and was shown to largely recapitulate the hallmarks of the human disease [27].

In addition to liver disease, a second late diabetic complication explored in this study is retinopathy. This is a disorder in which a decrease in the percentage of HbA1c was 25% efficient in preventing diabetic microvascular complications, suggesting that chronic hyperglycemia plays a critical role in DR. Likewise, reactive dicarbonyls are able to mimic early retinal changes in animal models [28]. IR or the MetS can cause occasional structural retinopathy, but much more frequent causes functional deficits, particularly at the venular site of the retinal vasculature, demonstrating that metabolic stress in the absence of overt hyperglycemia induces microvascular damage in a few cases [29]. Iron is known to damage the posterior retina (photoreceptors and retinal pigment epithelium), while in diabetes, early changes are found in the neurovascular unit. The evolution of diabetic microvascular damage reveals the formation of acellular occluded capillaries at its core, which is incited by pericyte loss as the long-standing confirmed hallmark [28,30].

In our previous work, we demonstrated that the db/db mouse model of IR and T2DM shows an "iron resistance" phenotype, whereby the liver, affected by NAFLD, is iron deficient despite increased plasma iron levels [31]. To reflect on the elevated hepatic iron content observed in patients with T2DM and thus to investigate the role of iron in hepatic complications and DR, we generated and analyzed a novel db/db mouse model with iron accumulation due to HH type 4.

2. MATERIALS AND METHODS

2.1. Experimental animals

Lean ($LepR^{db/wt}$) male mice were obtained from Harlan Laboratories and crossed with $Fpn^{wt/C326S}$ female mice to obtain the founders ($Fpn^{wt/C326S}$;$LepR^{db/wt}$ and $Fpn^{wt/wt}$;$LepR^{db/wt}$) used to generate the four experimental models herein described. Mice were housed at the SPF barrier of the Interfakultäre Biomedizinische Forschungseinrichtung (IBF) animal facility of the University of Heidelberg under a constant light–dark cycle and maintained on a standard mouse diet containing 200 ppm iron (LASQCdiet® Rod18) with ad libitum access to food and water. Diabetic heterozygous $Ins2^{Akita+/-}$ ($Ins2^{Akita}$) mice, purchased from Jackson Laboratory (Charles River Laboratories, Germany), were bred at the animal facility of the University Hospital Mannheim, Heidelberg University. Age-matched non-diabetic homozygous $Ins2^{Akita+/+}$ littermates served as control [32]. All animals were maintained following approval from the Animal Ethics Committee, in accordance with German Animal Welfare Act for the care and use of laboratory animals and the rules of the regulatory authorities in Baden-Württemberg (T-81/14, T-94/15).

2.2. Diabetes-related measurements

Blood glucose was measured using the Accu-Chek Aviva glucometer (Roche). Serum insulin was quantified in technical duplicate using the "Rat/Mouse insulin ELISA" (Millipore) according to manufacturer's instructions. Insulin concentration was extrapolated using a four parameter logistics standard curve. HbA1c levels have been measured

in HPLC and quantified as % of non-glycated hemoglobin, as previously described [33].

2.3. Quantitative RT-PCR

RNA was extracted from snap-frozen tissues using the Trizol reagent (Life technologies) and reverse transcribed using random hexamers and the RevertAid H Minus Reverse Transcriptase (Life technologies). SYBR green Real-Time PCR was performed with the ABI StepONE Plus System using the primers reported in Table S1. Relative mRNA expression was normalized to the *Actb* mRNA. Results were calculated using the Pfaffl method [34].

2.4. Western blotting

Protein lysates were obtained by homogenizing snap-frozen tissues in RIPA buffer supplemented with protease and phosphatase inhibitors (Roche Diagnostics) and quantified using the BCA protein assay according to manufacturer's instructions (Pierce). We subjected 50 μg of protein to western-blot analysis using 0.22 μm nitrocellulose membrane (Neolab) with the antibodies listed in Table S2. Western blot images were quantitatively acquired with the Vilber Lourmat Fusion-FX system.

2.5. Histology

Tissues were fixed for 24 h in 10% neutral buffered formalin (Sigma), dehydrated in ethanol gradients, paraffin embedded and sectioned at 3 μm on polylysine slides (Thermo scientific). Slides were rehydrated with decreasing percentage of ethanol solutions and subjected to stains.

For iron staining, slides were quenched with 3% H_2O_2 and treated for 20 min with Prussian Blue (Sigma Aldrich) followed by a 20 min incubation with 3,3′-diaminobenzidine (DAB) (Sigma Aldrich). Meyer's hematoxylin was used as counterstain.

For Masson's trichrome staining, slides were treated overnight with the Bourin's mordent solution (Roth). After washing, slides were treated for 5 min with Weigert's hematoxylin (Roth), 5 min with Biebrich Scarlet-Acid Fuchsine (Sigma Aldrich), 5 min with Phosphotungstic/Phosphomolybdic Acid Solution (Sigma Aldrich), 5 min with Aniline Solution (Sigma Aldrich) and 2 min with 1% acetic acid (Carl Roth).

For hematoxylin and eosin staining, slides were treated for 6 min with Mayer's Hematoxylin (Sigma Aldrich), rinsed in phosphate buffered saline, and incubated for 2 min in Eosin in acetic acid (Sigma Aldrich). After the stains, slides were dehydrated with ethanol gradients and mounted with Entellan (Sigma Aldrich). Digital images were acquired up to 40 × magnification with an automated slide scanner (Aperio - Leica biosystems)

2.6. Non-heme iron measurement

Tissue non-heme iron measurement was performed using the Bathophenanthroline method [35]. The iron concentration was normalized against the weight of the dry tissue.

2.7. Metabolite analysis

Hepatic glucose levels were measured by gas chromatography—mass spectrometry (GC—MS) at the Metabolomics Core Technology Platform of the University of Heidelberg and normalized against wet liver tissue weight.

2.8. Quantitative retinal morphometry

Quantitative retinal morphometry was performed on retinal digest preparations to evaluate numbers of pericytes (PC/mm^2 capillary area) and acellular capillaries (AC/mm^2 retinal area), according to established methods [36].

2.9. Statistical analyses

Results are shown as mean ± standard error of mean (SEM). Statistical analyses were performed using GraphPad Prism v8. Unless specified, 6 or more animals per group were used. Two-tailed Student's t-test was used and p-values <0.05 (*), <0.01 (**), <0.001 (***) and <0.0001 (****) are indicated.

3. RESULTS

3.1. Generation of a db/db mouse model with IR and iron overload

The db/db mouse is one of the most widely studied disease models of T2DM due to IR. The phenotype occurs due to a spontaneous mutation in the leptin receptor which causes polyphagy [37]. The liver of db/db mice is hallmarked by hepatic iron deficiency despite the presence of increased systemic iron levels [31]. To study phenotypic consequences of liver iron overload in db/db mice, as seen in patients with T2DM, we crossed db/db mice with Fpn p.C326S mice, a mouse model hallmarked by severe iron overload [27]. In total, four mouse models were generated and analyzed: lean control mice with normal iron status ($Lepr^{wt/db}$; $Fpn^{wt/wt}$), db/db mice ($Lepr^{db/db}$; $Fpn^{wt/wt}$), lean iron overloaded mice ($Lepr^{wt/db}$; $Fpn^{wt/C326S}$), and mice with iron overload on a db/db genetic background ($Lepr^{db/db}$; $Fpn^{wt/C326S}$).

At 30 weeks of age, db/db female mice compared to lean controls showed all the hallmarks of T2DM and the expected IR: hyperglycemia, hyperinsulinemia, and increased HbA1c. The body weight was dramatically increased, consistent with the polyphagic behavior of db/db mice (Figure 1A). The same alterations were detectable in iron-loaded db/db ($Lepr^{db/db}$; $Fpn^{wt/C326S}$) mice when compared with iron-loaded lean animals ($Lepr^{wt/db}$; $Fpn^{wt/C326S}$) (Figure 1A), suggesting that iron overload introduced by the Fpn p.C326S genetic background did not dramatically alter the features of IR detected in db/db mice (Figure 1A).

Similar results were obtained at 15 weeks of age in male and female animals. This indicates that even at a younger age and regardless of the gender, increased iron levels do not influence systemic diabetic hallmarks (Figure S1A,E).

3.2. The db/db genetic background alters systemic iron indices of mice with hereditary hemochromatosis type 4

We next focused our attention on the analysis of iron-related serum markers. Consistent with the iron-overload phenotype of lean $Fpn^{wt/C326S}$ mice, we observed higher serum iron levels than that of lean controls (Figure 1B) [27]. Surprisingly, the db/db genetic background dramatically enhances the amount of circulating iron levels by about 50% in 30 week-old mice and to 45% and 20% in male and female 15 week-old mice, respectively (Figures 1B, S1B, and S1F), demonstrating that the degree of serum iron accumulation is progressive with age.

Serum ferritin is a clinical marker of body iron status that is elevated in iron overload conditions. Consistently, lean $Fpn^{wt/C326S}$ mice show increased serum ferritin levels compared to lean controls (Figure 1B). The presence of the db/db genetic background reduces serum ferritin levels (comparison of lean $Fpn^{wt/C326S}$ and $Lepr^{db/db}$; $Fpn^{wt/C326S}$ mice). Importantly, ferritin levels in $Lepr^{db/db}$; $Fpn^{wt/C326S}$ mice were still significantly higher than that in $Lepr^{wt/db}$; $Fpn^{wt/C326S}$ mice, suggesting that these mice are able to increase tissue iron levels.

3.3. The db/db genetic background reduces hepatic iron levels and alters the iron-related molecular signature

The liver is the main iron storage organ and maintains systemic iron homeostasis by producing the iron regulatory hormone hepcidin. The

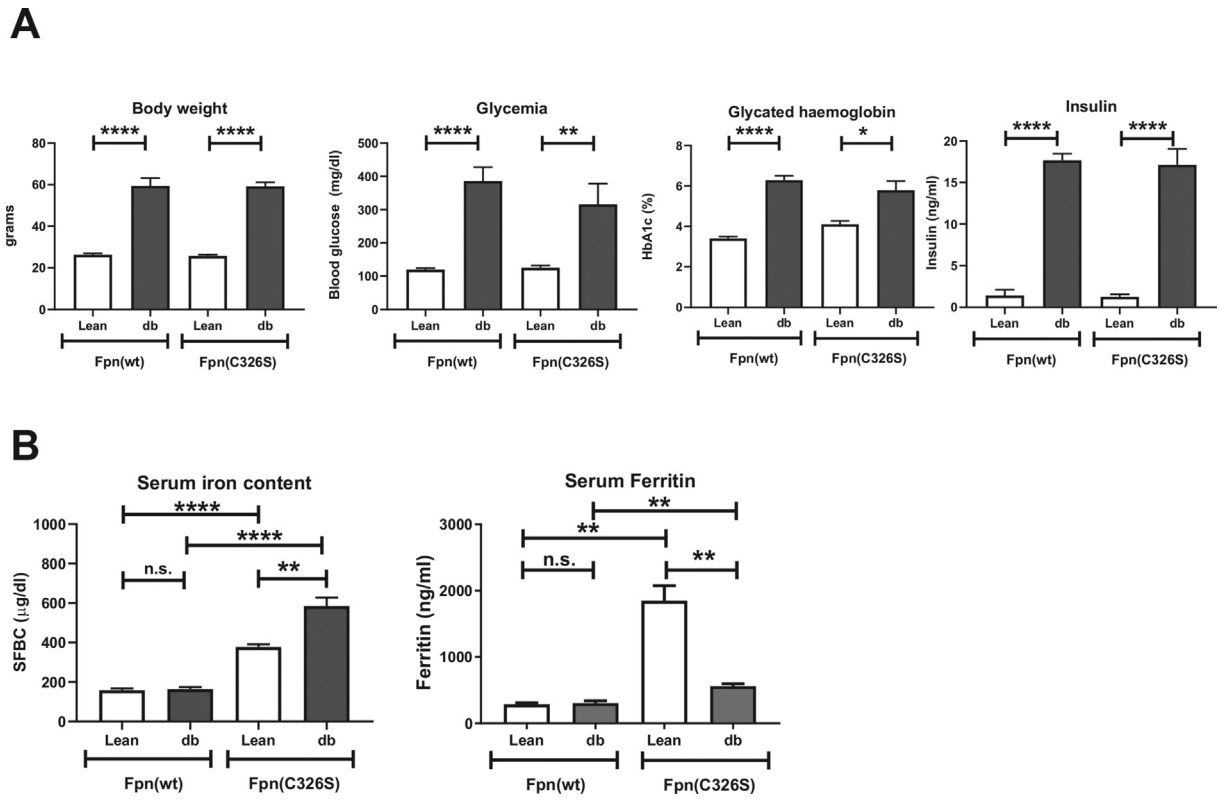

Figure 1: Diabetic and iron parameters in Lepr$^{db/db}$; Fpn$^{wt/C326S}$ mice. Biomarkers that hallmark type 2 diabetes (A) and iron-related parameters (B) were analyzed in 30-week-old female mice with the indicated genotype. (A) Body weight of mice (in grams), blood glycemia (mg/dL), glycated hemoglobin (HbA1c) and serum insulin (ng/ml) are shown. B) Serum iron content (µg/dL) and serum ferritin levels (ng/ml). All data are reported as mean ± SEM. Six or more mice per group were analyzed. Student's t-test p-value: *$p < 0.05$; **$p < 0.01$; ***$p < 0.001$; ****$p < 0.0001$.

liver further controls energy balance by storing glucose as glycogen; it is one of the few organs able to generate glucose via gluconeogenesis and, together with the adipocytes, it can synthetize fatty acids via *de novo* lipogenesis.

We subsequently analyzed the liver iron content. We showed reduced iron levels in both male and female 15 week old db/db mice (Figures S1C and S1G), confirming the "iron resistance" phenotype previously observed [31]. The hepatic iron resistance persisted at 30 weeks of age (Figure 2A–B). Interestingly, hepatic iron levels are also reduced in iron-loaded db/db (Lepr$^{db/db}$; Fpn$^{wt/C326S}$) compared to iron-loaded lean Lepr$^{wt/db}$; Fpn$^{wt/C326S}$ mice (Figures 2AB, S1C, and S1G).

Liver cells take up iron through the transferrin-bound iron importer transferrin receptor 1 (TfR1). We demonstrated increased mRNA expression of TfR1 in Lepr$^{db/db}$ animals irrespective of the presence of the Fpn p.C326S mutation (Figure 2C), whereby TfR1 mRNA likely is stabilized by intracellular iron deficiency via the iron responsive element/iron regulatory protein (IRE/IRP) system. Iron export from liver cells is mediated by the iron exporter ferroportin that shows increased mRNA expression in conditions of iron overload [27]. Ferroportin mRNA levels remain unaltered in Lepr$^{db/db}$ mice compared to lean controls (Figure 2D), whereby Fpn protein levels are decreased, consistent with reduced hepatic iron content (Figure 2E–F). This is consistent with the response of the IRE/IRP system in iron deficiency that represses ferroportin translation. Hepcidin-mediated degradation of ferroportin is unlikely involved as hepcidin mRNA levels are inappropriately low in the liver of Lepr$^{db/db}$ mice, even in the presence of iron accumulation due to the Fpn p.C326S genetic background (Figure 2G). Furthermore, Lepr$^{db/db}$; Fpn$^{wt/C326S}$ mice that are heterozygous for the Fpn p.C326S mutation that prevents hepcidin binding, would partially inhibit hepcidin-mediated ferroportin degradation. To explain low hepcidin mRNA expression, we next analyzed whether signals and pathways involved in regulating hepcidin transcription are altered. Hepcidin transcription is mainly regulated by two signaling pathways: the BMP/SMAD pathway, which controls the hepcidin response to iron and the IL-6/JAK/STAT3 pathway, which drives the hepcidin response to inflammation [38]. Hepatic BMP6 mRNA expression was reduced in db/db models irrespective of the Fpn p.C326S genetic background (Figure 2H). Consistently, mRNA expression of the BMP/SMAD target genes ID1, SMAD6, and ATOH8 were also downregulated (Figure 2I–K). Conversely, the inflammatory pathways seem unchanged as indicated by mRNA expression levels of the JAK/STAT downstream target SOCS3 (Figure 4E). Increased gluconeogenesis signals trigger an upregulation of the endoplasmic reticulum (ER) stress-related transcriptional factor CREBH in hepatocytes, whereby CREBH activates hepcidin transcription as a strategy to preserve iron stores upon starvation [39]. Herein, we showed that hepatic CREBH mRNA expression was unchanged (Figure 2L) suggesting that it does not act in a feedback loop to counteract decreased hepcidin expression.

Taken together, these results indicate that (1) the pathological consequences of the db/db genetic background cause reduced liver iron levels that are not explained by reduced Tfr1 or increased ferroportin expression levels. (2) Reduced liver iron levels, rather than increased circulating iron levels are sensed by the liver, as BMP6 and hepcidin

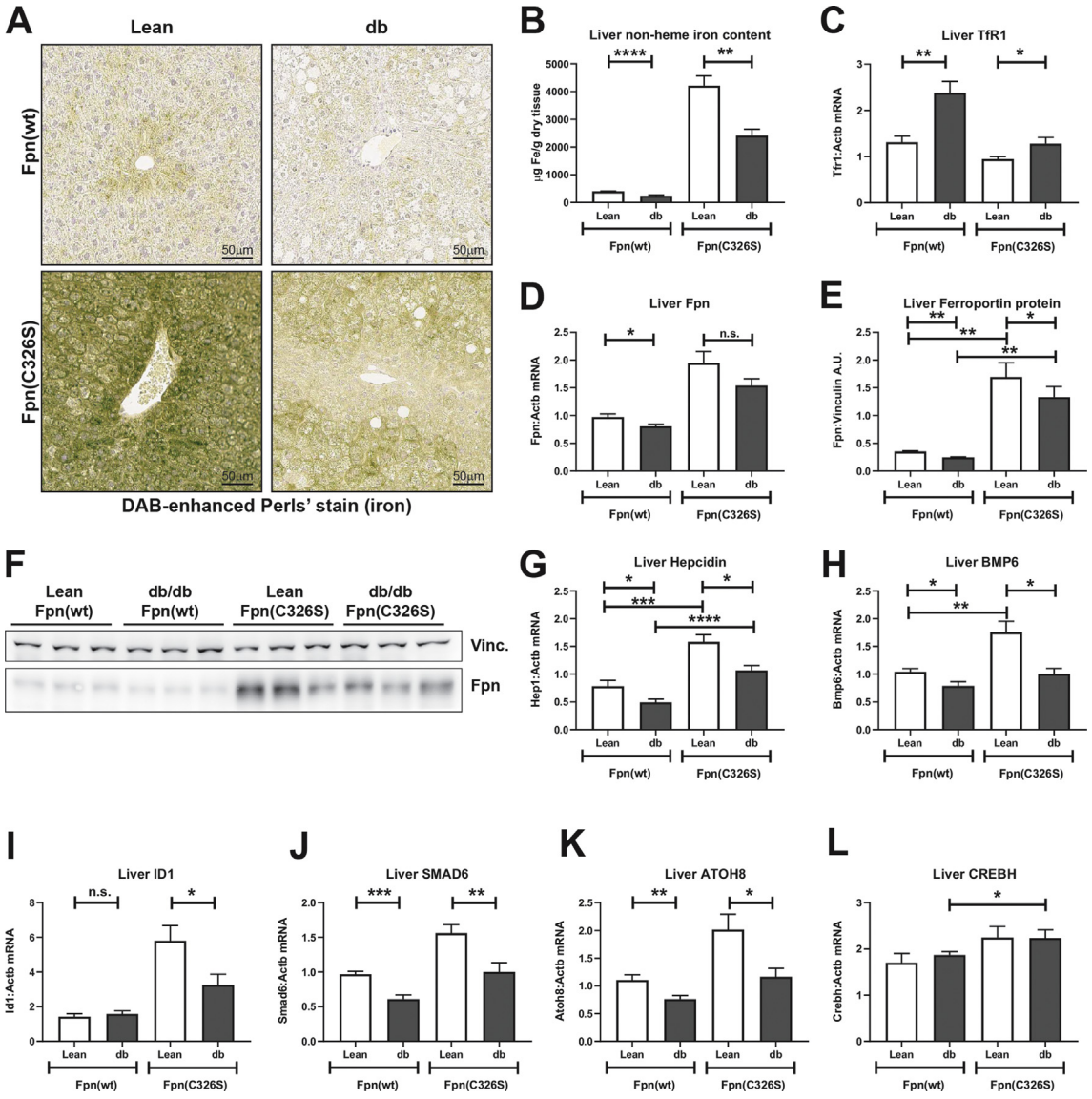

Figure 2: Analyses of iron-related parameters in the liver. A) DAB-enhanced Perls' iron staining of the liver. B) Quantification of the hepatic non-heme iron content normalized against dry tissue weight. C-D) Gene expression analysis of the iron transferrin-bound iron importer transferrin receptor (TfR)1 (C) and of the iron exporter ferroportin (D). E-F) Western blot analysis of the protein levels of the iron exporter Ferroportin normalized against the housekeeping gene Vinculin. G-K) Gene expression analysis of the iron regulatory hormone hepcidin (G), of the bone morphogenetic protein BMP6 (H), of the BMP/SMAD target genes ID1 (I), SMAD6 (J) and ATOH8 (K) and of the ER-stress related gene CREBH (L) Gene expression mRNA levels have been normalized against the housekeeping gene β-actin (ACTB). All data are reported as mean ± SEM. Six or more mice per group were analyzed. Student's t-test p-value: *$p < 0.05$; **$p < 0.01$; ***$p < 0.001$; ****$p < 0.0001$.

mRNA expression is diminished in accordance with the liver iron status. (3) The iron-related changes observed are unlikely a consequence of hyperglycemia in db/db mice (Figure S2D), as the $Ins2^{Akita}$ mouse model of insulinopenia with severe hyperglycemia does not show alterations in the hepatic iron content (Figure S2A), plasma hepcidin (Figure S2B), and plasma iron levels (Figure S2C).

We further demonstrated that the "iron resistant" phenotype is not limited to the liver. Analysis of the iron content of other organs such as the pancreas similarly showed reduced iron levels (Figures S3A and S3B). These findings raise the interesting question how the pathological features operational in $Lepr^{db/db}$ mice reduce the ability of the liver to accumulate high iron levels even in the presence of an iron overload phenotype in $Fpn^{wt/C326S}$ mice.

3.4. Liver iron accumulation affects IR

In $Lepr^{db/db}$ mice, polyphagia caused marked hepatic steatosis, indicative of NAFLD that is almost universally detected in patients affected by IR and T2DM. Upon inflammation and oxidative stress, NAFLD progresses to non-alcoholic steatohepatitis (NASH), which is associated with the worsening of IR. At 30-weeks of age, $Lepr^{db/db}$ female mice showed clear signs of steatosis, confirming NAFLD (Figure 3A). Masson's trichrome stain for collagen deposition excluded the presence of fibrosis, and thus NASH, in all the models analyzed here (Figure 3B). Furthermore, hematoxylin and eosin stain did not reveal hepatic inflammatory cell infiltration (Figure 3A). This is consistent with the lack of a local pro-inflammatory status of the liver, as shown by normal expression levels of the JAK/STAT3 target gene

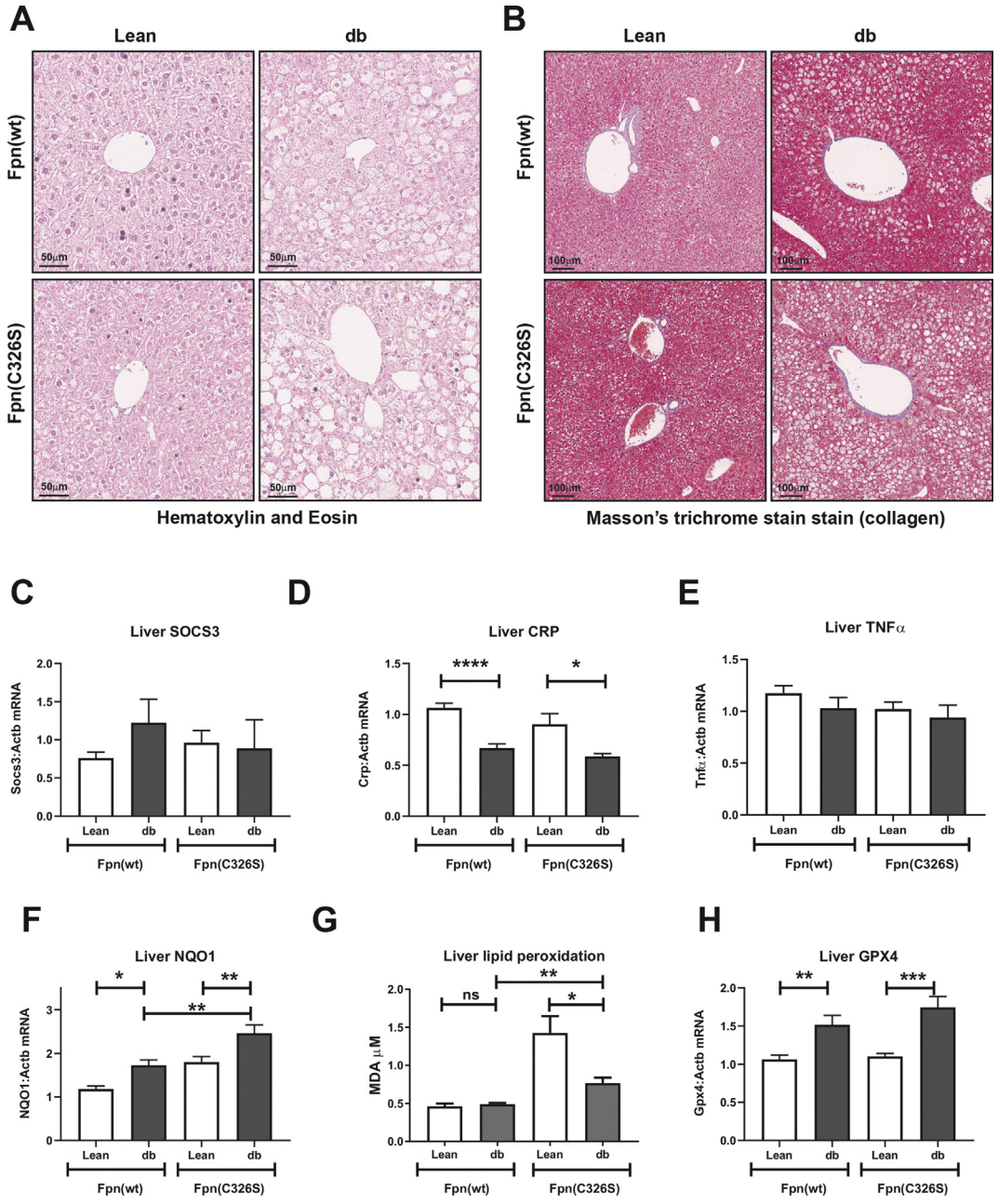

Figure 3: Characterization of hepatic NAFLD/NASH-related parameters. A-B) Hematoxylin & eosin to detect structural abnormalities and immune cell infiltration (A) and Masson's trichrome stain to detect collaged deposition (B) in livers of 30-week-old female mice with the genotypes indicated C-E). Analysis of the hepatic inflammatory status by measuring gene expression of the inflammatory-related gene SOCS3 (C), of the acute phase protein CRP (D) and of the pro-inflammatory cytokine TNFα (E). F—H) Analysis of hepatic oxidative stress by assessing the mRNA expression of the Nrf2 target gene Nqo1 (F), of lipid peroxidation via the TBARS assay (G) and mRNA expression of the lipid antioxidant enzyme glutathione peroxidase 4 (GPX4) (H). Gene expression values were normalized to the housekeeping gene β-actin (ACTB). Six or more mice per group were analyzed. All data are reported as mean ± SEM. Student's t-test p-value: *$p < 0.05$; **$p < 0.01$; ***$p < 0.001$; ****$p < 0.0001$.

SOCS3 (Figure 3C), the acute phase protein C-reactive protein (CRP) (Figure 3D) and of the pro-inflammatory cytokine TNFα (Figure 3E). In addition, the spleen is protected from inflammation, as shown by the unaltered mRNA expression of the pro-inflammatory interleukins IL6 and IL1β, of TNFα and of the inflammatory downstream target gene SOCS3 (Figure S4), excluding extra-hepatic production of inflammatory cytokines. NAFLD is hallmarked by increased oxidative stress that generates lipid peroxides. The transcription factor Nrf2 is activated by oxidative stress to orchestrate oxidative stress surveillance mechanisms. Consistently, Nqo1, an Nrf2 target gene, showed increased mRNA expression in $Lepr^{db/db}$; $Fpn^{wt/wt}$ mice and even higher levels in iron-loaded $Lepr^{db/db}$; $Fpn^{wt/C326S}$ mice (Figure 3F). The presence of oxidative stress was further demonstrated by elevated lipid peroxidation, as identified by the increased production of malondialdehyde (Figure 3G) and increased mRNA expression of Glutathione peroxidase 4 (GPX4) in $Lepr^{db/db}$; $Fpn^{wt/C326S}$ mice, a selenoprotein that acts as antioxidant by reducing lipid peroxides to lipid alcohols (Figure 3H).

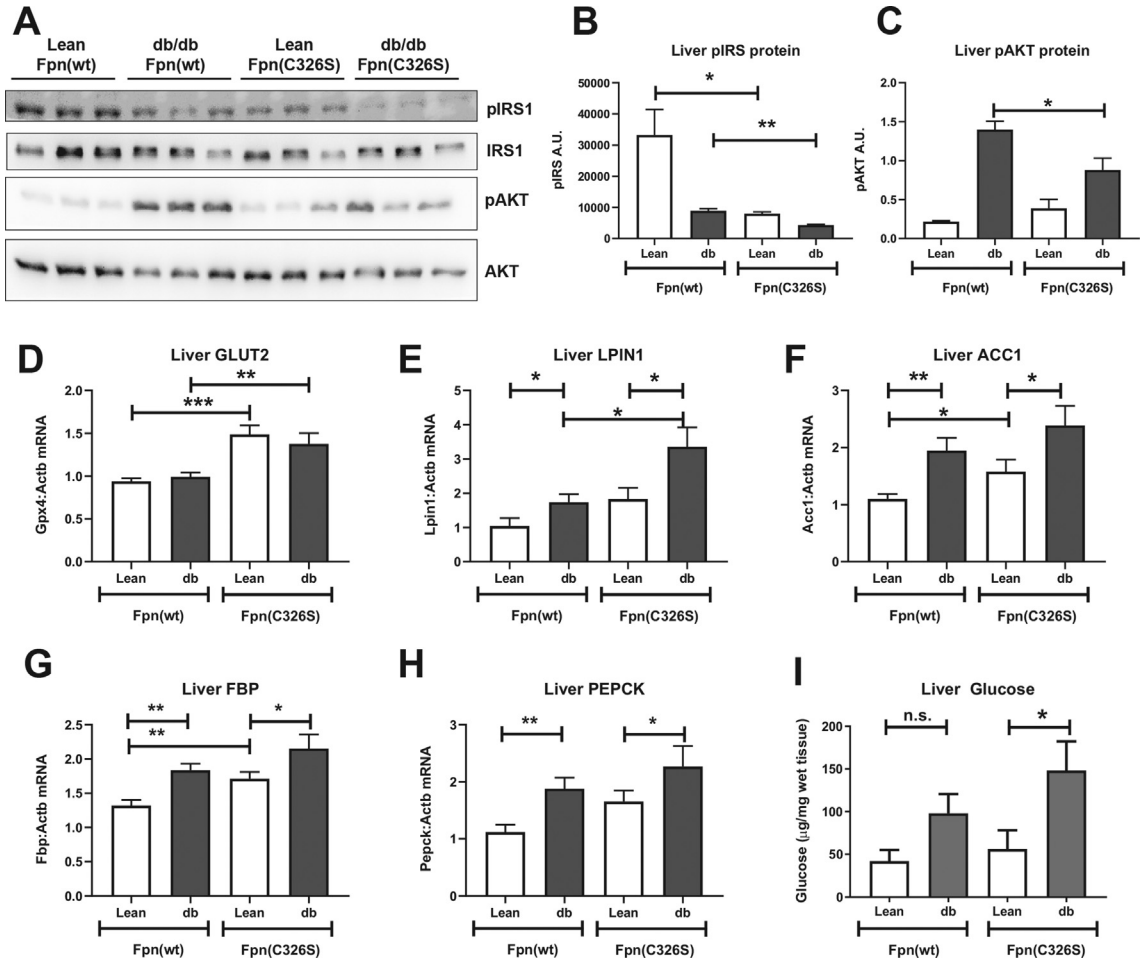

Figure 4: Analysis of hepatic diabetes-related parameters. A-C) Western blot protein analysis of phosphorylated and total Insulin Receptor Substrate 1 (pIRS and IRS, respectively), and of the Protein Kinase B (AKT) and its phosphorylated form pAKT. D-H) Gene expression analysis of the glucose transporter GLUT2 (D), of the *de novo* lipogenesis-related genes LPIN1 (E) and ACC1 (F) and of gluconeogenesis-related genes FBP (G) and PEPCK (H). I) Hepatic free glucose levels were analyzed by GC—MS and normalized against wet tissue weight. Gene expression values were normalized to the housekeeping gene β-actin (ACTB). Six or more mice per group were analyzed. All data are reported as mean ± SEM. Student's t-test p-value: *$p < 0.05$; **$p < 0.01$; ***$p < 0.001$; ****$p < 0.0001$.

We next focused our attention on the analysis of the insulin-related pathways. Consistent with IR in $Lepr^{db/db}$ mice, we observed decreased levels of phospho-Insulin Receptor Substrate-1 (pIRS1). Interestingly, lean iron overloaded mice ($Lepr^{wt/db}$;$Fpn^{wt/C326S}$) also show a strong decrease in pIRS1, which is strongly enhanced in iron-loaded $Lepr^{db/db}$; $Fpn^{wt/C326S}$ mice (Figure 4A—B). Consistent with the higher degree of IR, $Lepr^{db/db}$; $Fpn^{wt/C326S}$ mice show lower levels of the insulin/pIRS1 downstream target protein phospho-AKT (pAKT), when compared to $Lepr^{db/db}$ mice (Figure 4A,C). We further showed that iron overload may affect glucose uptake by upregulating mRNA expression of the insulin-independent glucose transporter GLUT2 (Figure 4D). IR and increased glucose uptake cause profound alterations in liver metabolism that are associated with increased gluconeogenesis and elevated *de novo* lipogenesis. Consistently, $Lepr^{db/db}$ mice show increased mRNA expression of Lpin and Acc1, two genes involved in the *de novo* synthesis of triglycerides (Figure 4J—K). An additive increase of Lpin and Acc1 mRNA expression is observed in $Lepr^{db/db}$; $Fpn^{wt/C326S}$ mice, suggesting that iron overload potentially aggravates triglyceride synthesis. Similarly, genes affecting gluconeogenesis, Fructose-Bisphosphatase-1 (FBP) and Phosphoenolpyruvate Carboxykinase-1 (PEPCK) show increased mRNA expression levels (Figure 4E—H). Importantly, increased gluconeogenesis results in higher free hepatic glucose levels in $Lepr^{db/db}$ mice, whereby the concentration is even higher in iron-loaded $Lepr^{db/db}$; $Fpn^{wt/C326S}$ mice (Figure 4I).

Taken together, these data show that iron accumulation in the liver enhances the generation of hepatic IR and downstream effects on glucose and lipid metabolism.

3.5. The Fpn p.C326S mutation does not aggravate IR in the diabetic adipose tissue

Visceral obesity is one of the components of MetS and is strictly related to the onset of T2DM. Analysis of the iron content in visceral adipose tissue (VAT) of $Lepr^{db/db}$ animals revealed a minor increase in iron levels that is only mildly enhanced in iron-loaded $Lepr^{db/db}$; $Fpn^{wt/C326S}$ mice (Figure 5A). At the molecular level, the alteration of VAT iron content was reflected by increased heme oxygenase 1 mRNA expression (Figure 5B) despite the fact that Nrf2 redox surveillance is not significantly activated (Figure 5C). Interestingly, VAT expressed mRNA of the iron exporter ferroportin, which was mildly increased in iron-loaded $Lepr^{db/db}$; $Fpn^{wt/C326S}$ mice (Figure 5D).

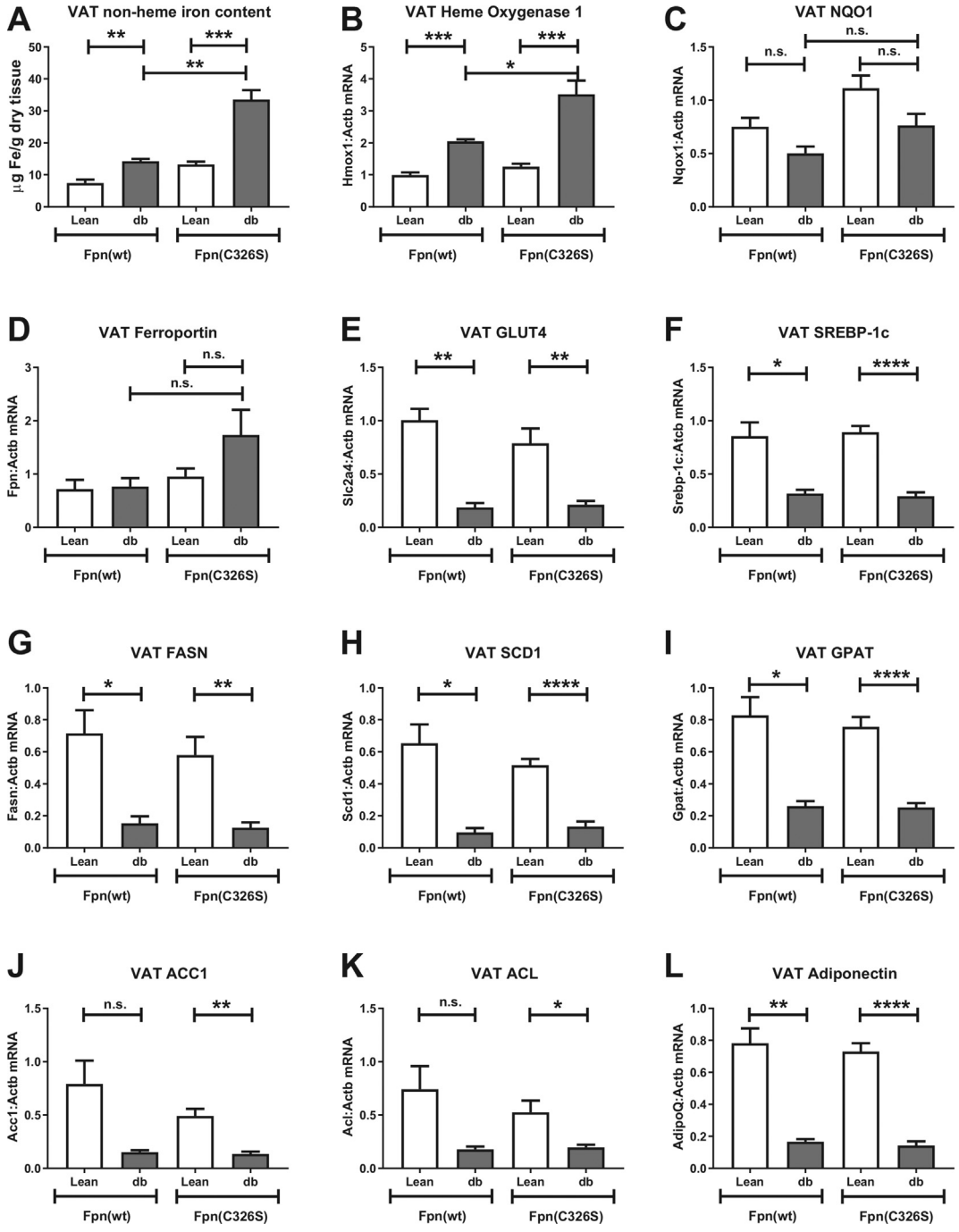

Figure 5: Iron- and diabetic-related characterization of the visceral adipose tissue. A) Quantification of the visceral adipose tissue (VAT) non-heme iron content normalized against dry tissue weight. B-D) Gene expression analysis of the iron and oxidative stress-related genes heme oxygenase 1 (B) Nqo1 (C) and of the iron exporter Ferroportin (D). E-K) Gene expression analysis of the glucose transporter GLUT4 (E), of the insulin-related transcription factor Srebp-1c (F) and of Srebp-1c target genes FASN (G), SCD1 (H), GPAT (I), ACC1 (J) and ACL (K). Gene expression analysis of the adipokine Adiponectin (L). Gene expression values were normalized to the housekeeping gene β-actin (ACTB). All data are reported as mean ± SEM. Student's t-test p-value: *$p < 0.05$; **$p < 0.01$; ***$p < 0.001$; ****$p < 0.0001$.

IR caused a decrease in the expression of the glucose transporter Glut4 and of the sterol regulatory element binding protein Srebp-1c [40,41] (Figure 5E—F). Consistently, mRNA expression of Srebp-1c target genes involved in *de novo* lipogenesis, such as fatty acid synthase (FAS), stearoyl-CoA desaturase-1 (SCD1), glycerol-3-phosphate acyl-transferase (GPAT), acetyl-CoA carboxylase (ACC) and ATP-citrate lyase (ACL) was decreased (Figure 5G—K). As expected, IR reduced the expression of the insulin sensitizer adipokine Adiponectin [42] (Figure 5L). Mild iron accumulation in the VAT of iron-loaded $Lepr^{db/db}$; $Fpn^{wt/C326S}$ mice does not further modify the expression of these insulin-related target genes (Figure 5E—L). This suggests that the degree of iron accumulation reached in our models is not sufficient to aggravate IR in the visceral adipose tissue, contrasting results obtained in the liver.

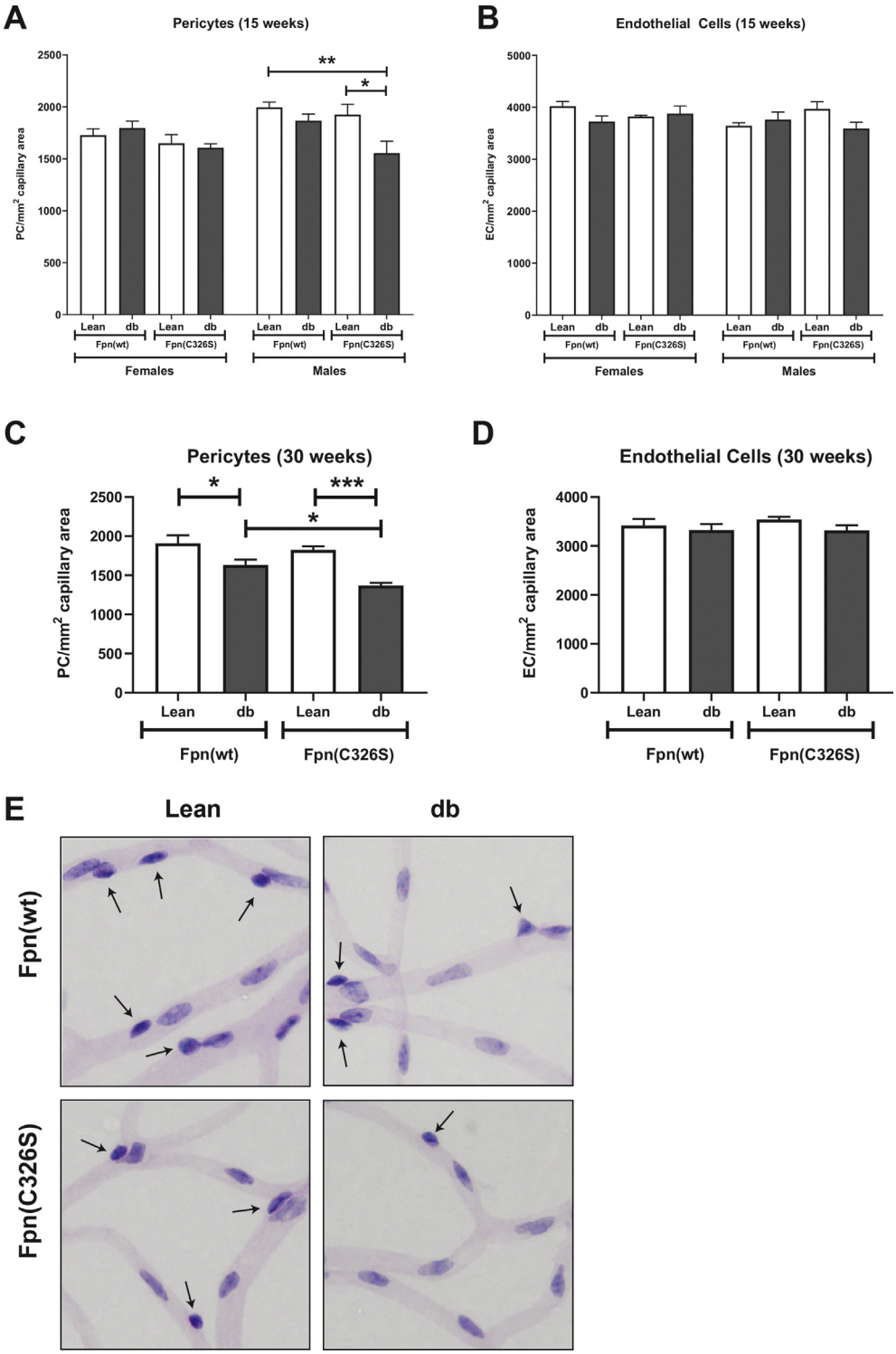

Figure 6: Increased pericyte loss hallmarks iron-loaded Lepr$^{db/db}$ mice. A-B) Analysis of pericyte (A) and endothelial cell (B) number, normalized against the capillary area, in the eyes of 15-week old mice with the genotype and the gender indicated. C-D) Characterization of pericyte (C) and endothelial cells (D) in the eyes of 30-week old male mice. E) Representative histological analysis of the microvasculature of the retina in 30-week-old male mice with the genotype indicated. All data are reported as mean ± SEM. Six or more mice per group were analyzed. Student's t-test p-value: *p $<$ 0.05; **p $<$ 0.01; ***p $<$ 0.001; ****p $<$ 0.0001.

3.6. Iron overload enhances the diabetic-related pericyte loss in the eyes

Beyond the liver, Lepr$^{db/db}$ mice showed features of diabetic late complications in other organs. Diabetic retinopathy is one of the most common diabetic late complications and a leading cause of blindness in the western world [43]. It is considered as a microvascular-related disease since, at an early stage, sustained hyperglycemia, oxidative stress, or reactive metabolites induce apoptosis of the pericytes,

structural components of the microvessels, causing breakage of the blood-retinal-barrier.

At 15 weeks of age, $Lepr^{db/db}$ mice show normal pericyte and endothelial cell numbers, irrespective of the gender. This indicates that at this early stage, the retinal microvasculature remains unaffected. However, 15 week-old iron-loaded and obese $Lepr^{db/db}$; $Fpn^{wt/C326S}$ male mice of the same age showed a mild but significant pericyte loss (Figure 6A—B). At 30 weeks of age, pericyte loss is evident also in $Lepr^{db/db}$ mice. This effect is aggravated by iron-accumulation in $Lepr^{db/db}$; $Fpn^{wt/C326S}$ mice, indicating that elevated systemic iron levels can worsen the early stages of DR observed in $Lepr^{db/db}$ mice (Figure 6C,E). Of note, at this age, the number of endothelial cells remains unaffected (Figure 6D—E).

4. DISCUSSION

Almost 70% of patients affected by IR and T2DM display fatty acid accumulation in the liver, a condition defined as NAFLD [44]. Hepatic accumulation of free fatty acids causes saturation of mitochondrial β-oxidation resulting in hydrogen peroxide formation. Oxidative stress may further arise from iron accumulation, as excess free ferrous iron catalyzes the conversion of hydrogen peroxide to hydroxyl radicals, the most potent members of ROS [21]. Indeed, increased hepatic iron stores and hyperferritinemia are frequently observed in steatotic patients and have been associated with more severe liver damage [16]. Two large studies conducted in NAFLD patients indicated that iron accumulation either predominantly in hepatocytes [16] or reticuloendothelial macrophages [17] is responsible for development of fibrosis. To date, direct evidence for the role of iron in aggravating hepatic IR and T2DM is still missing. To address this clinically relevant question in a murine disease model of steatosis, IR, T2DM and iron accumulation, we crossed $Lepr^{db/db}$ mice with a genetic model of hereditary hemochromatosis type 4 (Fpn p.C326S).

The first result of our analysis is that increased systemic iron accumulation does not affect obesity, hyperinsulinemia, hyperglycemia, and increased HbA1c normally observed in T2DM $Lepr^{db/db}$ animals (Figures 1A, S1A, and S1E). More surprisingly, we illustrated that the db/db genotype modifies systemic hemochromatosis-related iron parameters. At 15 weeks of age and independent of the gender, we observed strongly increased serum iron levels in $Lepr^{db/db}$; $Fpn^{wt/C326S}$ mice that exceeded the already high levels in mice with hereditary hemochromatosis type 4 ($Fpn^{wt/C326S}$ mice) (Figures S1B and S1F), a phenotype that persisted in aged mice (Figure 1B). Serum iron levels were also elevated in younger (15 week-old) $Lepr^{db/db}$ mice compared to lean wild-type controls (Figures S1B and S1F) [31]. This was not the case in 30 week old $Lepr^{db/db}$ mice, suggesting that aging modifies some of the mechanisms underlying elevated serum iron levels. Elevated systemic iron levels are likely explained by an inability of the liver (and other organs) to accumulate iron in $Lepr^{db/db}$ and iron-loaded obese $Lepr^{db/db}$; $Fpn^{wt/C326S}$ mice. This hypothesis is corroborated by the reduced serum ferritin levels, a marker of body iron stores in $Lepr^{db/db}$; $Fpn^{wt/C326S}$ mice (Figure 1B).

The pancreas in $Fpn^{wt/C326S}$ mice accumulates iron exclusively in the exocrine compartment that lacks expression of the iron exporter ferroportin (Figure S3A) [27]. Thus, reduction of the pancreatic iron content in $Lepr^{db/db}$; $Fpn^{wt/C326S}$ mice compared to $Fpn^{wt/C326S}$ lean controls (Figure S3B) is unlikely explained by an increased iron efflux but rather by decreased iron uptake. Similarly, in the liver, ferroportin protein levels are reduced in $Lepr^{db/db}$; $Fpn^{wt/C326S}$ mice compared to that in $Fpn^{wt/C326S}$ lean controls (Figure 2D—F) likely due to IRE/IRP mediated repression of Fpn mRNA translation under conditions of reduced iron availability (Figure 2A,B). Consistently, an additional IRP target gene, the iron importer TfR1 is increased due to mRNA stabilization. Overall, this indicates that the liver adequately responds to the differential iron content.

The inability of tissues to accumulate iron seems to be specific for the phenotype of the db/db genetic background. $Ins2^{Akita}$ mice, a widely used model of type 1 diabetes mellitus, show hyperglycemia and high levels of reactive metabolites, similar to db/db mice, but tissue iron levels remain unaltered, even after six months of hyperglycemia (Figure S2). Lower hepatic iron levels have also been observed in a murine model of obesity due to dietary high fat administration. However, unlike the models analyzed here that show increased systemic iron levels, the high fat diet model shows reduced plasma iron content most likely due to impaired dietary iron uptake [45]. This suggests that a combination of features typical of T2DM such as obesity, steatosis, or hyperinsulinemia/IR that manifest themselves in the db/db genetic background may be responsible for reduced tissue iron uptake.

An additional interesting aspect of this study is the gene expression pattern of hepcidin. mRNA expression of this key regulatory iron hormone does not follow systemic iron levels but rather mirrors the hepatic iron content (Figures 1B, 2B, and 2G). The hepcidin response to increased iron levels is chiefly dependent on the production of the bone morphogenetic protein BMP6 by the liver sinusoidal endothelial cells. Endothelial BMP6 is released into the space of Disse and acts in a paracrine way on hepatocytes to regulate hepcidin transcription via the BMP/SMAD pathway. In $Lepr^{db/db}$; $Fpn^{wt/C326S}$ mice BMP6 production is reduced, consistent with iron levels in the liver, strengthening the hypothesis that BMP6 is produced in response to the hepatic iron content rather than systemic iron levels.

Despite the resistance of iron uptake in $Lepr^{db/db}$; $Fpn^{wt/C326S}$ mice, in absolute terms these mice show higher systemic and hepatic iron levels compared to $Lepr^{db/db}$ mice. Consistently, systemic ferritin levels are increased. This provides us with a bona-fide model to study the effects of increased iron levels, mirroring DIOS, on the pathogenesis and progression of IR and T2DM. Iron accumulation in the liver triggers an oxidative stress response, as indicated by increased mRNA expression of the Nrf2 target gene Nqo1 (Figure 3F). In addition, oxidative stress further increases the levels of lipid peroxidation, in particular in $Lepr^{db/db}$; $Fpn^{wt/C326S}$ mice that are hallmarked by fatty acid deposition (Figure 3G). Iron-induced lipid peroxidation is one of the key features of a novel form of cell death called ferroptosis. GPX4 is the only enzyme that can reduce lipid peroxides to lipid alcohol, thus inhibiting ferroptosis. Gene expression analysis revealed an increase in GPX4 transcript levels exclusively in $Lepr^{db/db}$ mice, irrespective of the iron status (Figure 3H). This suggests that free fatty acid deposition triggers GPX4 production as a mechanism to limit potential toxic consequences of increased lipid peroxidation.

It was proposed that increased oxidative stress together with a local pro-inflammatory status trigger the progression of NAFLD to NASH and aggravates IR causing T2DM [46]. NASH is hallmarked by fibrosis. However, histological analysis of the livers of the mouse models analyzed failed to show accumulation of collagen (Figure 3B), immune cell infiltration, or structural abnormalities aside from steatosis (Figure 3A). These results complement observations in other disease models of hereditary hemochromatosis (e.g. $Hjv^{-/-}$ and $Hfe^{-/-}$ mice) maintained on a high fat diet, in which the hepatic iron overload does not induce a NAFLD to NASH progression [47].

A possible explanation for a lack of progression to NASH may be due to a lack of hepatic inflammation, as indicated by the unchanged expression of the JAK/STAT target gene suppressor of cytokine signaling 3 (SOCS3), of the acute phase protein CRP and of the pro-

inflammatory cytokine TNFα (Figure 3C–E). Epidemiological studies have shown that in the steatotic liver, iron accumulation in Kupffer cells is associated with increased fibrosis [48,49]. Iron accumulation in macrophages causes a switch toward a pro-inflammatory status [22]. However, Fpn p.C326S mice and patients with hereditary hemochromatosis do not accumulate iron in macrophages due to the stabilization of ferroportin on the cell surface and increased iron export. Consistently, the spleen of $Lepr^{db/db}$; $Fpn^{wt/C326S}$ mice shows reduced iron levels (Figures S4A and S4B) and splenic mRNA expression of inflammatory mediators are not elevated (Figure S4D). Thus, uncontrolled iron export from macrophages may explain a lack of inflammation and hepatic fibrosis in iron-loaded $Lepr^{db/db}$; $Fpn^{wt/C326S}$ mice.

In support of this hypothesis, $Lepr^{db/db}$ animals maintained on a high iron diet [50] showed increased hepcidin levels that trap iron in macrophages causing a pro-inflammatory phenotype. Interestingly, NASH was observed in a murine model of dietary iron overload. Our finding may have implications for patients with hereditary hemochromatosis, a wide-spread disorder in the Caucasian population with a carrier frequency of 1 in 8 that may be protected from tissue inflammation due to the failure to accumulate iron in macrophages.

A further important finding of this study is that iron accumulation in hepatocytes aggravates hepatic IR. IRS-1 is a key component of the insulin signaling pathway. It functions as an adapter to transduce the signal from the insulin-activated insulin receptor to the downstream PI3K-AKT kinases [51]. $Lepr^{db/db}$ mice, hallmarked by IR, show decreased IRS-1 phosphorylation in the liver compared to lean controls. Interestingly, $Fpn^{wt/C326S}$ mice also show decreased phospho-IRS-1 levels, an effect that is aggravated in $Lepr^{db/db}$; $Fpn^{wt/C326S}$ mice. As a consequence, AKT activation is decreased, when compared to $Lepr^{db/db}$ mice (Figure 4A–C), indicating that iron overload triggers a higher degree of hepatic IR, which in turn may be responsible for a gluconeogenesis molecular signature and increased hepatic free glucose levels (Figure 4I). In addition, iron overload increases mRNA expression of the insulin-independent glucose transporter GLUT2 (Figure 4D). The combination of IR and higher glucose uptake via GLUT2 likely will increase *de novo* lipogenesis. These results complement findings from experiments in cultured cells and observations in patients. It was shown previously that iron chelation in HepG2 hepatoma cell lines increases insulin receptor activity and Akt phosphorylation while iron supplementation shows the opposite effect [52]. Consistently, some NAFLD patients subjected to venesection, a typical intervention in patients affected by iron overload, show an improvement of IR and glycemic control [53], a finding that was not substantiated by a meta-analysis [54].

Analogous to the liver, we analyzed whether iron overload in visceral adipose tissue (VAT) aggravates IR. IR in adipose tissue triggers a switch from *de novo* lipogenesis to lipolysis and alters the production and secretion of adipokines involved in insulin sensitivity, such as adiponectin. The liver is particularly susceptible to these changes as it is connected directly downstream the visceral adipose tissue via the portal vein through which it receives free fatty acids and adipokines. We showed that iron levels are very low in the VAT of lean $Lepr^{wt/db}$ mice and only mildly increased in $Lepr^{db/db}$ and $Lepr^{db/db}$; $Fpn^{wt/C326S}$ animals despite the dramatic increase in serum iron levels (Figures 1B and 5A). This mild increase in iron levels does not aggravate the typical IR signature observed in the VAT of $Lepr^{db/db}$ animals, indicated by low mRNA expression of the glucose transporter GLUT4, of the *de novo* lipogenesis-related transcription factor Srebp1c, of genes involved in fatty acid synthesis (Figure 5G–K) and of the insulin sensitizing hormone Adiponectin.

In contrast to our results in $Lepr^{db/db}$; $Fpn^{wt/C326S}$ mice, exposure of wild-type mice to a high iron diet induces iron accumulation in the VAT, decreased adiponectin production and IR [55,56]. We speculate that in wild-type mice degradation of ferroportin in response to iron-induced hepcidin levels in adipocytes may allow for iron accumulation, a response prevented by the p.C326S mutation in ferroportin in $Lepr^{db/db}$; $Fpn^{wt/C326S}$ mice. Thus, differential ferroportin sensitivity to hepcidin may explain why in the dietary model adipocytes accumulate 10 times more iron compared to controls [56] while in this study we could detect only a mild increase in iron levels (Figure 5A).

This hypothesis is corroborated by the results obtained in adipocyte-specific Fpn knock-out mice, which show VAT iron accumulation and reduced adiponectin expression [55]. Of note, $Hfe^{-/-}$ mice, a disease model of HH type 1 that shows less severe iron overload due to mild hepcidin suppression [57], is hallmarked by decreased fasting glucose levels, adipocyte iron deficiency, and increased adiponectin production [55]. Conversely, more severe models of HH such as the Fpn p.C326S [27], $Hjv^{-/-}$ [58] or $Hamp^{-/-}$ [59] show a normal glucose/insulin tolerance test or fasting glucose levels. We explain this by different degrees of systemic iron levels and Fpn stabilization, causing alterations in the adipocyte iron efflux/influx ratio and thus different adipocyte iron content. Different VAT iron levels may thus be responsible of the outcome in terms of adipocyte IR.

DR is the most commonly identified diabetic complication and is the major cause of visual loss in working-age populations [43]. The initial phases of this disorder are hallmarked by the degeneration of the retinal microvasculature causing increased permeability, capillary occlusion, and blood-retinal barrier dysfunction. This leads to the "leaking" of the vessels generating diabetic macular edema and impaired vision. Pericytes and endothelial cells are the two main cellular constituents in the retinal microvasculature. Pericytes have both a secretory and a contractile component and structurally support the endothelium of the microvessels. In T2DM, several factors could be responsible of DR. Hyperglycemia, increased reactive metabolites and oxidative stress in pericytes induces apoptosis leading to pericyte loss and microvasculature dysfunction. Importantly, even though hyperglycemia is an established factor for DR, this late complication can also occur in patients that show minor changes in HbA1c levels [10]. Pericyte loss was previously shown in $Lepr^{db/db}$ mice associated with IR and T2DM, causing a change in the ratio of endothelial cells to pericytes in the capillaries of the retina [60].

Of note, systemic iron overload moderately aggravates T2DM-related vascular damage as indicated by pericyte loss over time. Interestingly, only the combination of oxidative stress and hyperglycemia caused an early significant dropout of pericytes, while later, the damage was aggravated with the combination. While the observation that high glucose causes retinopathy is in agreement with many prior studies, the finding that iron overload causes more damage is novel. It is known that iron can cause structural abnormalities of the posterior retina, but not to the inner circulatory part which is the target of hyperglycemic changes in diabetes. Interestingly, photoreceptor damage can cause pericyte damage in models of ciliopathy-associated retinopathy, but this was not observed in the model of iron overload, suggesting that mechanisms of systemic oxidative stress such as the diabetic iron overload model are different from tissue specific challenge through prolonged photoreceptor degeneration [61].

Altogether, our results show that increased iron levels in $Lepr^{db/db}$ mice can aggravate hepatic IR and DR. This raises the possibility that pharmacological strategies that limit iron accumulation could be used, together with the classic anti-diabetic drugs, to ameliorate IR and diabetic late complications.

AUTHOR CONTRIBUTIONS

S.A and K.M generated and characterized the $Lepr^{db/db}$; $Fpn^{wt/C326S}$ mouse models. T.F. measured the HbA1c levels. E.H. measured the free glucose levels in the liver. R.Q. performed western blot experiments. A.S. and H.P.H provided livers and plasma of the $Ins2^{Akita}$ mice and analyzed the retinas of the $Lepr^{db/db}$; $Fpn^{wt/C326S}$ animals. S.A. and M.U.M. wrote the manuscript. M.U.M. and P.N. supervised the project. All authors critically reviewed the manuscript.

ACKNOWLEDGEMENTS

This study was supported by the German Research Foundation [DFG - SFB1118].

CONFLICT OF INTEREST

The authors have no conflict of interest relevant to this study to declare.

APPENDIX A. SUPPLEMENTARY DATA

Supplementary data to this article can be found online at https://doi.org/10.1016/j.molmet.2021.101235.

REFERENCES

[1] Alberti, K.G., Eckel, R.H., Grundy, S.M., Zimmet, P.Z., Cleeman, J.I., Donato, K.A., et al., 2009. Harmonizing the metabolic syndrome: a joint interim statement of the International Diabetes Federation Task Force on Epidemiology and Prevention; National Heart, Lung, and Blood Institute; American Heart Association; World Heart Federation; International Atherosclerosis Society; and International Association for the Study of Obesity. Circulation 120(16):1640–1645.

[2] O'Neill, S., O'Driscoll, L., 2015. Metabolic syndrome: a closer look at the growing epidemic and its associated pathologies. Obesity Reviews 16(1):1–12.

[3] Ervin, R.B., 2009. Prevalence of metabolic syndrome among adults 20 years of age and over, by sex, age, race and ethnicity, and body mass index: United States, 2003-2006. National Health Statistics Report(13):1–7.

[4] Ford, E.S., 2005. Prevalence of the metabolic syndrome defined by the International Diabetes Federation among adults in the U.S. Diabetes Care 28(11):2745–2749.

[5] Saklayen, M.G., 2018. The global epidemic of the metabolic syndrome. Current Hypertension Reports 20(2):12.

[6] Scholze, J., Alegria, E., Ferri, C., Langham, S., Stevens, W., Jeffries, D., et al., 2010. Epidemiological and economic burden of metabolic syndrome and its consequences in patients with hypertension in Germany, Spain and Italy; a prevalence-based model. BMC Public Health 10:529.

[7] Han, T.S., Lean, M.E., 2016. A clinical perspective of obesity, metabolic syndrome and cardiovascular disease. JRSM Cardiovascular Disease 5, 2048004016633371.

[8] Wagner, R., Heni, M., Tabak, A.G., Machann, J., Schick, F., Randrianarisoa, E., et al., 2021. Pathophysiology-based subphenotyping of individuals at elevated risk for type 2 diabetes. Nature Medicine 27(1):49–57.

[9] Ismail-Beigi, F., Craven, T., Banerji, M.A., Basile, J., Calles, J., Cohen, R.M., et al., 2010. Effect of intensive treatment of hyperglycaemia on microvascular outcomes in type 2 diabetes: an analysis of the ACCORD randomised trial. Lancet 376(9739):419–430.

[10] Selvin, E., Ning, Y., Steffes, M.W., Bash, L.D., Klein, R., Wong, T.Y., et al., 2011. Glycated hemoglobin and the risk of kidney disease and retinopathy in adults with and without diabetes. Diabetes 60(1):298–305.

[11] Brown, A., Reynolds, L.R., Bruemmer, D., 2010. Intensive glycemic control and cardiovascular disease: an update. Nature Reviews Cardiology 7(7):369–375.

[12] Williams, C.D., Stengel, J., Asike, M.I., Torres, D.M., Shaw, J., Contreras, M., et al., 2011. Prevalence of nonalcoholic fatty liver disease and nonalcoholic steatohepatitis among a largely middle-aged population utilizing ultrasound and liver biopsy: a prospective study. Gastroenterology 140(1):124–131.

[13] Loomba, R., Abraham, M., Unalp, A., Wilson, L., Lavine, J., Doo, E., et al., 2012. Association between diabetes, family history of diabetes, and risk of nonalcoholic steatohepatitis and fibrosis. Hepatology 56(3):943–951.

[14] Lonardo, A., Bellentani, S., Argo, C.K., Ballestri, S., Byrne, C.D., Caldwell, S.H., et al., 2015. Epidemiological modifiers of non-alcoholic fatty liver disease: focus on high-risk groups. Digestive and Liver Disease 47(12):997–1006.

[15] Gastaldelli, A., 2010. Fatty liver disease: the hepatic manifestation of metabolic syndrome. Hypertension Research 33(6):546–547.

[16] Valenti, L., Fracanzani, A.L., Bugianesi, E., Dongiovanni, P., Galmozzi, E., Vanni, E., et al., 2010. HFE genotype, parenchymal iron accumulation, and liver fibrosis in patients with nonalcoholic fatty liver disease. Gastroenterology 138(3):905–912.

[17] Nelson, J.E., Wilson, L., Brunt, E.M., Yeh, M.M., Kleiner, D.E., Unalp-Arida, A., et al., 2011. Relationship between the pattern of hepatic iron deposition and histological severity in nonalcoholic fatty liver disease. Hepatology 53(2):448–457.

[18] Dongiovanni, P., Fracanzani, A.L., Fargion, S., Valenti, L., 2011. Iron in fatty liver and in the metabolic syndrome: a promising therapeutic target. Journal of Hepatology 55(4):920–932.

[19] Deugnier, Y., Bardou-Jacquet, E., Laine, F., 2017. Dysmetabolic iron overload syndrome (DIOS). Presse Medicale 46(12 Pt 2):e306–e311.

[20] Muckenthaler, M.U., Rivella, S., Hentze, M.W., Galy, B., 2017. A red carpet for iron metabolism. Cell 168(3):344–361.

[21] Altamura, S., Muckenthaler, M.U., 2009. Iron toxicity in diseases of aging: Alzheimer's disease, Parkinson's disease and atherosclerosis. Journal of Alzheimers Disease 16(4):879–895.

[22] Vinchi, F., Costa da Silva, M., Ingoglia, G., Petrillo, S., Brinkman, N., Zuercher, A., et al., 2016. Hemopexin therapy reverts heme-induced proinflammatory phenotypic switching of macrophages in a mouse model of sickle cell disease. Blood 127(4):473–486.

[23] Vinchi, F., Porto, G., Simmelbauer, A., Altamura, S., Passos, S.T., Garbowski, M., et al., 2020. Atherosclerosis is aggravated by iron overload and ameliorated by dietary and pharmacological iron restriction. European Heart Journal 41(28):2681–2695.

[24] Nemeth, E., Tuttle, M.S., Powelson, J., Vaughn, M.B., Donovan, A., Ward, D.M., et al., 2004. Hepcidin regulates cellular iron efflux by binding to ferroportin and inducing its internalization. Science 306(5704):2090–2093.

[25] Sham, R.L., Phatak, P.D., West, C., Lee, P., Andrews, C., Beutler, E., 2005. Autosomal dominant hereditary hemochromatosis associated with a novel ferroportin mutation and unique clinical features. Blood Cells Molecules and Diseases 34(2):157–161.

[26] Sham, R.L., Phatak, P.D., Nemeth, E., Ganz, T., 2009. Hereditary hemochromatosis due to resistance to hepcidin: high hepcidin concentrations in a family with C326S ferroportin mutation. Blood 114(2):493–494.

[27] Altamura, S., Kessler, R., Grone, H.J., Gretz, N., Hentze, M.W., Galy, B., et al., 2014. Resistance of ferroportin to hepcidin binding causes exocrine pancreatic failure and fatal iron overload. Cell Metabolism 20(2):359–367.

[28] Hammes, H.P., 2018. Diabetic retinopathy: hyperglycaemia, oxidative stress and beyond. Diabetologia 61(1):29–38.

[29] Mattern, J., Lammert, A., Otto, M., Hammes, H.P., 2017. Retinopathy in an obesity WHO III cohort: prevalence and risk factors. British Journal of Ophthalmology 101(11):1550–1554.

[30] Baumann, B.H., Shu, W., Song, Y., Sterling, J., Kozmik, Z., Lakhal-Littleton, S., et al., 2019. Liver-specific, but not retina-specific, hepcidin knockout causes retinal iron accumulation and degeneration. American Journal Of Pathology 189(9):1814–1830.

[31] Altamura, S., Kopf, S., Schmidt, J., Muedder, K., da Silva, A.R., Nawroth, P.P., et al., 2017. Uncoupled iron homeostasis in type 2 diabetes. Journal of Molecular Medicine.

[32] Maresch, C.C., Stute, D.C., Fleming, T., Lin, J., Hammes, H.P., Linn, T., 2019. Hyperglycemia induces spermatogenic disruption via major pathways of diabetes pathogenesis. Scientific Reports 9(1):13074.

[33] Ekim Ustunel, B., Friedrich, K., Maida, A., Wang, X., Krones-Herzig, A., Seibert, O., et al., 2016. Control of diabetic hyperglycaemia and insulin resistance through TSC22D4. Nature Communications 7:13267.

[34] Pfaffl, M.W., 2001. A new mathematical model for relative quantification in real-time RT-PCR. Nucleic Acids Research 29(9):2002—2007.

[35] Torrance, J.D., Bothwell, T.H., 1968. A simple technique for measuring storage iron concentrations in formalinised liver samples. South African Journal of Medical Sciences 33(1):9—11.

[36] Dietrich, N., Hammes, H.P., 2012. Retinal digest preparation: a method to study diabetic retinopathy. Methods in Molecular Biology 933:291—302.

[37] Hummel, K.P., Dickie, M.M., Coleman, D.L., 1966. Diabetes, a new mutation in the mouse. Science 153(3740):1127—1128.

[38] Muckenthaler, M.U., 2008. Fine tuning of hepcidin expression by positive and negative regulators. Cell Metabolism 8(1):1—3.

[39] Vecchi, C., Montosi, G., Garuti, C., Corradini, E., Sabelli, M., Canali, S., et al., 2014. Gluconeogenic signals regulate iron homeostasis via hepcidin in mice. Gastroenterology 146(4):1060—1069.

[40] Kouidhi, S., Berrhouma, R., Rouissi, K., Jarboui, S., Clerget-Froidevaux, M.S., Seugnet, I., et al., 2013. Human subcutaneous adipose tissue Glut 4 mRNA expression in obesity and type 2 diabetes. Acta Diabetologica 50(2):227—232.

[41] Kim, J.B., Sarraf, P., Wright, M., Yao, K.M., Mueller, E., Solanes, G., et al., 1998. Nutritional and insulin regulation of fatty acid synthetase and leptin gene expression through ADD1/SREBP1. Journal of Clinical Investigation 101(1):1—9.

[42] Kadowaki, T., Yamauchi, T., Kubota, N., Hara, K., Ueki, K., Tobe, K., 2006. Adiponectin and adiponectin receptors in insulin resistance, diabetes, and the metabolic syndrome. Journal of Clinical Investigation 116(7):1784—1792.

[43] Wang, W., Lo, A.C.Y., 2018. Diabetic retinopathy: pathophysiology and treatments. International Journal of Molecular Sciences 19(6).

[44] Adams, L.A., Angulo, P., 2007. Role of liver biopsy and serum markers of liver fibrosis in non-alcoholic fatty liver disease. Clinics in Liver Disease 11(1):25—35 viii.

[45] Sonnweber, T., Ress, C., Nairz, M., Theurl, I., Schroll, A., Murphy, A.T., et al., 2012. High-fat diet causes iron deficiency via hepcidin-independent reduction of duodenal iron absorption. The Journal of Nutritional Biochemistry 23(12): 1600—1608.

[46] Masarone, M., Rosato, V., Dallio, M., Gravina, A.G., Aglitti, A., Loguercio, C., et al., 2018. Role of oxidative stress in pathophysiology of nonalcoholic fatty liver disease. Oxidative Medicine and Cellular Longevity 2018:9547613.

[47] Wagner, J., Fillebeen, C., Haliotis, T., Charlebois, E., Katsarou, A., Mui, J., et al., 2019. Mouse models of hereditary hemochromatosis do not develop early liver fibrosis in response to a high fat diet. PloS One 14(8):e0221455.

[48] Kowdley, K.V., Belt, P., Wilson, L.A., Yeh, M.M., Neuschwander-Tetri, B.A., Chalasani, N., et al., 2012. Serum ferritin is an independent predictor of histologic severity and advanced fibrosis in patients with nonalcoholic fatty liver disease. Hepatology 55(1):77—85.

[49] Tacke, F., Zimmermann, H.W., 2014. Macrophage heterogeneity in liver injury and fibrosis. Journal of Hepatology 60(5):1090—1096.

[50] Handa, P., Morgan-Stevenson, V., Maliken, B.D., Nelson, J.E., Washington, S., Westerman, M., et al., 2016. Iron overload results in hepatic oxidative stress, immune cell activation, and hepatocellular ballooning injury, leading to nonalcoholic steatohepatitis in genetically obese mice. American Journal of Physiology - Gastrointestinal and Liver Physiology 310(2):G117—G127.

[51] White, M.F., 2002. IRS proteins and the common path to diabetes. American Journal of Physiology. Endocrinology and Metabolism 283(3):E413—E422.

[52] Facchini, F.S., Hua, N.W., Stoohs, R.A., 2002. Effect of iron depletion in carbohydrate-intolerant patients with clinical evidence of nonalcoholic fatty liver disease. Gastroenterology 122(4):931—939.

[53] Valenti, L., Fracanzani, A.L., Dongiovanni, P., Bugianesi, E., Marchesini, G., Manzini, P., et al., 2007. Iron depletion by phlebotomy improves insulin resistance in patients with nonalcoholic fatty liver disease and hyperferritinemia: evidence from a case-control study. American Journal of Gastroenterology 102(6):1251—1258.

[54] Murali, A.R., Gupta, A., Brown, K., 2018. Systematic review and meta-analysis to determine the impact of iron depletion in dysmetabolic iron overload syndrome and non-alcoholic fatty liver disease. Hepatology Research 48(3):E30—E41.

[55] Gabrielsen, J.S., Gao, Y., Simcox, J.A., Huang, J., Thorup, D., Jones, D., et al., 2012. Adipocyte iron regulates adiponectin and insulin sensitivity. Journal of Clinical Investigation 122(10):3529—3540.

[56] Dongiovanni, P., Ruscica, M., Rametta, R., Recalcati, S., Steffani, L., Gatti, S., et al., 2013. Dietary iron overload induces visceral adipose tissue insulin resistance. American Journal Of Pathology 182(6):2254—2263.

[57] Herrmann, T., Muckenthaler, M., van der Hoeven, F., Brennan, K., Gehrke, S.G., Hubert, N., et al., 2004. Iron overload in adult Hfe-deficient mice independent of changes in the steady-state expression of the duodenal iron transporters DMT1 and Ireg1/ferroportin. Journal of Molecular Medicine (Berlin) 82(1):39—48.

[58] Huang, F.W., Pinkus, J.L., Pinkus, G.S., Fleming, M.D., Andrews, N.C., 2005. A mouse model of juvenile hemochromatosis. Journal of Clinical Investigation 115(8):2187—2191.

[59] Ramey, G., Faye, A., Durel, B., Viollet, B., Vaulont, S., 2007. Iron overload in Hepc1(-/-) mice is not impairing glucose homeostasis. FEBS Letters 581(5): 1053—1057.

[60] Midena, E., Segato, T., Radin, S., di Giorgio, G., Meneghini, F., Piermarocchi, S., et al., 1989. Studies on the retina of the diabetic db/db mouse. I. Endothelial cell-pericyte ratio. Ophthalmic Research 21(2):106—111.

[61] Feng, Y., Wang, Y., Li, L., Wu, L., Hoffmann, S., Gretz, N., et al., 2011. Gene expression profiling of vasoregression in the retina–involvement of microglial cells. PloS One 6(2):e16865.

